Dual-mechanism estrogen receptor inhibitors expand the repertoire of anti-hormone therapy for breast cancer

Jian Min[1,2]*, Jerome C. Nwachukwu[3]*, Sathish Srinivasan[3], Erumbi S. Rangarajan[3], Charles C. Nettles[3], Charles Min[3], Valeria Sanabria Guillen[4], Yvonne Ziegler[4], Shunchao Yan[4,5], Kathryn E. Carlson[1], Yingwei Hou[1], Sung Hoon Kim[1], Scott Novick[6], Bruce D. Pascal[7], Rene Houtman[8], Patrick R. Griffin[3,6], Tina Izard[3], Benita S. Katzenellenbogen[4], John A. Katzenellenbogen[1]*, Kendall W. Nettles[3]*

[1]Department of Chemistry, Cancer Center and University of Illinois at Urbana-Champaign, Urbana IL 61801, USA

[2] State Key Laboratory of Biocatalysis and Enzyme Engineering, Hubei Collaborative Innovation Center for Green Transformation of Bio-Resources, Hubei Key Laboratory of Industrial Biotechnology, School of Life Sciences, Hubei University, Wuhan 430062, China

[3] Department of Integrative Structural and Computational Biology, The Scripps Research Institute, Jupiter, FL 33458, USA

[4] Department of Molecular and Integrative Physiology, Cancer Center and University of Illinois at Urbana-Champaign, Urbana IL 61801, USA

[5] Department of Oncology, Shengjing Hospital of China Medical University, Shenyang, Liaoning Province, 110022, P. R. China

[6] Department of Molecular Medicine, The Scripps Research Institute, Jupiter, FL 33458, USA

[7] Omics Informatics LLC, 1050 Bishop St. #517, Honolulu, HI, 96813, USA

[8] Precision Medicine Lab, 5349 AB Oss, The Netherlands

*Contributed equally

Address Correspondence to:

Dr. Kendall W. Nettles

Email: knettles@scripps.edu

Chemistry: Dr. John A. Katzenellenbogen

Email: jkatzene@illinois.edu

ABSTRACT

Tamoxifen and fulvestrant are currently two major approved estrogen receptor-α (ER)-targeted therapies for breast cancer, but resistance to their antagonistic actions often develops. Efforts to improve ER-targeted therapies have relied upon a single mechanism, where ligands with a single side chain on the ligand core that extends outward from the ligand binding pocket to directly displace helix (h)12 in the ER ligand-binding domain (LBD), blocking the LBD interaction with transcriptional coactivators that drive proliferation. Here, we describe ER inhibitors that block estrogen-induced proliferation through two distinct structural mechanisms by combining a side chain *for direct antagonism* with a bulky chemical group that causes *indirect antagonism* by distorting structural epitopes inside the ligand binding pocket. These dual-mechanism ER inhibitors (DMERIs) fully antagonize the proliferation of wild type ER-positive breast cancer cells and cells that have become resistant to tamoxifen and fulvestrant through activating ER mutations and de novo mechanisms such as overactive growth factor signaling. Conformational probing studies highlight marked differences that distinguish the dual mechanism inhibitors from current standard of care single-mechanism antiestrogens, and crystallographic analyses reveal that they disrupt the positioning of h11 and h12 in multiple ways. Combining two chemical targeting approaches into a single ligand thus provides a flexible platform for next generation ER-targeted therapies.

INTRODUCTION

The estrogen receptor-α (ER) plays a critical role in breast cancer where it functions as a major driver of tumor growth in ~70% of breast cancers. While the suppression of ER function with endocrine therapy by inhibiting estrogen production with aromatase inhibitors (AIs) or by blocking ER activity with antiestrogens is initially quite effective (*1, 2*), many ER-positive breast cancers recur in forms that have become resistant to standard-of-care AIs and/or antiestrogens, while de novo resistance also occurs. In these resistant cases, however, it is possible that antiestrogens of novel design might still prove effective because most of the tumor cells still express ER (*3*).

Currently, there are two types of approved antiestrogens. Tamoxifen (*4*) and its newer generation analogs, raloxifene, bazedoxifene and lasofoxifene, are called selective estrogen receptor modulators (SERMs) due to their bone-sparing activity (*5*), and they all contain a similar aromatic ring that we call the E-ring (named with respect to the 4 rings of steroids that are lettered A-D, **Fig. S1A–B**). The E ring is attached to an aminoalkyl side chain via through a two-carbon ether that exits from the ligand binding pocket and interacts on the receptor surface with a single H-bond at Asp351 (**Fig. S1A**); in this stabilized position, the side chain controls the displacement of transcriptional coactivators that drive proliferation (*6-10*).

Fulvestrant, the only approved ER antagonist for treatment of tamoxifen or AI-resistant breast cancer (*11*), and other full antagonists such as RU 58,668, are termed selective estrogen receptor downregulators (SERDs), because they also reduce ER levels, although this effect may not be required for their antagonist activity (*12-14*). Both of these SERDs contain an extended terminal fluorine-substituted alkyl sulfinyl or sulfonyl sidechain (**Fig. S1B**). Adequate dosing of fulvestrant is, however, limited by its poor pharmacokinetic properties and requires delivery by large, painful intramuscular injections.

Newer, orally active SERDs under clinical development have acrylate side chains (**Fig. S1C**), again using a 2-carbon linker to the carboxyl group, akin to that of the SERMs (*12, 15-20*). Both FDA-approved SERMs and potential oral SERD replacements for fulvestrant contain a single, carefully positioned aminoalkyl or acrylate side chain that *directly* repositions helix 12 (h12) in the ER ligand binding domain (LBD), disrupting the surface binding site for transcriptional coactivators that drive proliferative gene expression, thus operating by a *direct antagonism* mechanism of action.

Here, we present dual -mechanism estrogen receptor inhibitors, a new class of ER antagonists that combine a side chain for *direct antagonism* with a bulky chemical group that causes *indirect antagonism* by distorting epitopes inside the ligand binding pocket. Indirect antagonism independently drove full antagonism, enabling the direct antagonist side chain to adopt new structural and functional roles associated with new conformations of the receptor. They were effective against constitutively active mutant ERs, and in a *de novo* resistance model, overexpression of the epidermal growth factor receptor (EGFR), which causes tamoxifen resistance and is associated with a worse clinical outcome (*21, 22*). The dual targeting approach produced compounds with SERM-like properties and also full antagonists/SERDs. Some of the latter showed efficacy greater than fulvestrant in a new structure-based design model of SERM/SERD agonist activity, highlighting the flexibility of platform for the production of compounds that are effective against endocrine therapy-resistant breast cancer.

RESULTS

Dual-mechanism inhibitors produce full antagonism of breast cancer cell proliferation irrespective of their side chain structure and site of substitution

Indirect antagonists produce a range of activity profiles by interfering with the docking of h12 across h3 and h5, which is required for formation of the surface binding site for transcriptional coactivator complexes, called Activation Function-2 (AF-2). Starting from a bulky oxabicyclic scaffold that contained aromatic rings corresponding to the A and E rings of other ER ligands (**Fig. S1A–C**), we appended a sulfonamide linker to prepare a 7-oxabicyclo[2.2.1]heptene sulfonamide (OBHS-N) core scaffold, as illustrated by the parental OBHS-N compound **13** (**Fig. 1A**). We previously showed that **13** was a full antagonist SERD, equivalent to fulvestrant in inhibiting proliferation of breast cancer cells with WT ER (*23*). By shifting the position of h11 by 2.4 Å, **13** blocked the interaction between the N-terminus of h3 and the C-terminus of h11 (**Fig. S1D**), and disrupted the agonist binding site for h12 against h11 (**Fig. S1E**). However, compounds in this parental series were not effective against the constitutively active mutants of ERα that drive treatment resistant disease, including the Y537S-ER mutation that adds an H-bond to Asp351 that stabilizes h12 in the agonist conformer (**Fig. S1E**) (*23, 24*), counteracting the ligand-dependent destabilization of h12 by tamoxifen as well.

Importantly, the sulfonamide substitution that drives indirect antagonism contains another aromatic ring that we call the F-ring, which provides an alternate position, 4.4 Å away from the E-ring, from which to launch a direct agonist side chain into an unexplored structural space in ER antagonism (**Fig. 1A**). This allowed us to evaluate two novel pharmacophores for ER antagonism: 1) Combining indirect antagonism with the canonical direct antagonism from the E-ring; and 2) combining direct and indirect antagonism through the F-ring.

We prepared OBHS-N compounds with the traditional ether-two carbon-aminoalkyl side chain attached to the E-ring ([E]-OC_2-piperidine (**16**)) or the F-ring ([F]-OC_2-piperidine (**19**)) (**Datasheet S1, Supplemental Methods**). Both of these compounds inhibited the growth of MCF-7 breast cancer cells with greater efficacy than 4OHT (the active 4-hydroxy metabolite of tamoxifen) and equivalent efficacy to fulvestrant (**Fig. 1B**), but **16** was more potent than **19** (with 11 nM and 97 nM IC_{50}s, respectively). We obtained X-ray crystal structures of these compounds in complex with the ER LBD in the antagonist conformer, where h12 was displaced from the agonist position and flipped onto the AF2 surface to block coactivator binding (**Fig. S1F**). As expected, the [E]-OC_2-Pip side chain of **16** displaced h12 and formed a tight H-bond with h3 Asp351, whereas the F-ring shifted h11 2.4 Å away from the position required for optimal agonist activity (**Fig. 1C, Fig. S1F**).

To our surprise, the side chain of [F]-OC_2-Pip (**19**) did not point towards h12, but instead exited between h8 and h11, where it is stabilized by H-bonds with h11 His524 (**Fig. 1D, Fig. S1G**). In this novel orientation, the antagonist side chain position pushed h11 towards the agonist position of h12 by 1.4 Å, which is also expected to prevent formation of the agonist conformer and is consistent with its strong antagonism. This represents a new form of indirect antagonism, which was possible due to the presence of two rotatable bonds in the sulfonamide, allowing the F-ring to adopt multiple positions relative to the core (**Fig. S1H**). Examples of this were observed again in our series of crystal structures described below, and likely contributes to the unusual activity profiles of these ligands.

TO find other novel structural conformations from combining direct and indirect antagonism, we explored a wider range of side chains (**Fig. S2A–H**), including the one found in RU 58,668 ([E]-RU (**14**)) and the acrylate found in orally active SERDs ([E]-Acr (**22**)). We tested side chains attached to the F-ring, including [F]-RU (**15**) and [F]-Acr (**23**), and also explored new side chains outside those historically required for antagonism, including an acrylate-ester ([F]-AcrEster (**21**)), piperidines with 3- or 4-carbon linkers ([E]-

157 OC_3-Pip (**17**)), ([E]-OC_4-Pip (**18**)), and ([F]-OC_3-Pip (**20**)), and a simple benzyl substitution
158 (([E]-Bn (**24**)) or ([F]-Bn (**25**). Notably, all of the compounds showed efficacy comparable
159 to fulvestrant, except for the acrylate-substituted compounds (**22** and **23**) that had μM
160 IC_{50}s and did not saturate the receptor (**Fig. 1E, Fig. S2E**). These broad antagonist
161 efficacies differ markedly from previous work by us (*25*) and others (*12, 26-28*) on single-
162 mechanism ER inhibitors, where subtle changes in the single side chain results in widely
163 divergent outcomes in terms of efficacy, highlighting the more restricted chemical and
164 structural requirements needed for effective single-mechanism inhibition of ERα activity.
165 Here, the compounds with non-canonical side chains profiled as full antagonists similar to
166 the parental compound (**13, Fig. 1A**), which was as efficacious as fulvestrant in inhibiting
167 breast cancer cell proliferation.

168 The side chains did, however, produce compounds covering almost 4 logs of IC_{50}
169 values, which is important because resistance mechanisms include both a loss of efficacy
170 and also substantial losses in potency. This loss of potency associated with resistance is
171 clinically important as fulvestrant is dose limited by its poor pharmacokinetics, which is
172 associated with its lack of clinical response (*29*). With the Roussel side chains (**14** and **15**)
173 and the acrylates (**22** and **23**), the F-ring substitutions gave higher potencies, whereas E-
174 ring substitutions with piperidine (**16**–**20**) or benzyl (**24** and **25**) side chains led to higher
175 potencies. With the F-ring piperidines, the 3-carbon linker **20** had ~1 log higher potency
176 than the 2-carbon linker **19**, while the acrylate ester **21** was almost 2 logs higher potency
177 than the corresponding acrylate **23** (**Fig. 1E**). Because all of the OBHS-N compounds are
178 racemates, we used chiral HPLC to resolve two of the compounds **24** and **15**, and we
179 found that one enantiomer of each (**29** from **24**, and **27** from **15**) accounted for essentially
180 all of their affinity and cellular activity. These preferred enantiomers, **29** and **27**, had
181 antiproliferative IC_{50}s of 3 and 0.3 nM, respectively (**Fig. 1E, Fig. S2G–H**).

To verify on-target mechanism of action, we inhibited cell growth with a subset of the compounds and showed full pharmacological reversal with increasing doses of estradiol (**Fig. S2I**). We also showed that the compounds completely antagonized E2-induced expression of the ERα-target gene, *GREB1* (**Fig. S2J**), demonstrating antagonism comparable to fulvestrant. Notably, the compounds also had no effect on proliferation of MDA-MB-231 cells, a triple-negative breast cancer cell line that lacks ER (**Fig. S2K**), again supporting ER specificity.

Dual mechanism inhibitor side chains determined both SERM and SERD activity profiles

To probe whether the side chains supported SERM or SERD like activities of the ligands, we first tested several compounds for effects on degradation of ERα, and found that direct antagonist side chain determined whether compounds displayed SERM- or SERD-like properties. [E]-Bn (**24**) and the higher affinity enantiomer of [F]-RU, [F]-RU-Ent2 (**27**) were efficient degraders (**Fig. 1F**). These effects were reversed by 4-hydroxytamoxifen (4OHT) or the proteasome inhibitor, MG132, demonstrating on-target mechanism of action through proteasomal degradation (**Fig. S3A**). In contrast, the compounds with piperidine side chains were more SERM-like with either minimal effects on receptor stability (**14**, **17**, and **19**), or some stabilization of the receptor (**16** and **20**, **Fig. 1F**).

To further probe for the cell-type selective activity that define SERMs, we tested the compounds in a reporter assay in HepG2 liver cells, a context in which tamoxifen displays significant agonist activity through the amino-terminal AF-1 domain of ER (*30*). We found that all the compounds with piperidine containing SERM side chains (**16-20**) showed some cell-type specific agonist activity, while the degraders **24** and **27** were full antagonists (**Fig. 1G, Fig. S3B**). Thus, the dual mechanism inhibitor approach can produce compounds

with SERM- or SERD-like properties that are highly efficacious and contain non-canonical side chains.

To test whether the compounds were effective against the constitutively active Y537S-ER, we tested the compounds in a luciferase reporter assay. All compounds displayed less potent IC_{50} values compared to the MCF-7 cell proliferation data or luciferase reporter assay with WT ER (**Fig. S4** vs **Fig S2A–H** or **Fig. S3B**). Several of the more potent piperidines were efficacious (**16-19, Fig. 1H**), as were the [F]-AcrEster and [F]-RU compounds (**21** and **27, Fig. S4**). It is noteworthy that compounds with lower efficacy did not saturate the receptor at the highest doses tested (**Fig. S4**), suggesting that this loss of efficacy may have been driven by the lower potency of these compounds in this resistance model. Addition of the direct antagonist side chain enabled efficacy in the Y537S resistance model, including the non-traditional F-ring substituted compounds and piperidines with longer linkers.

Compound-specific coregulator peptide interaction profiles reveal that dual-mechanism inhibitors induce unique ER solution structures

We examined the interaction of full-length ER-WT, or the constitutively active ER-Y537S that drives treatment resistant metastatic disease, with a library of 154 peptides using the Microarray Assay for Realtime Coregulator-Nuclear receptor Interaction (MARCoNI) assay as a probe for solution structure (*12, 31*). Hierarchical clustering of the FRET data from 19 compounds x 154 peptides is shown in **Fig. 2A**, demonstrating a clustering of E2-induced peptide interactions (*Cluster 3*) that were strongly dismissed by 4OHT, fulvestrant, and the full antagonist SERDs, GDC-0810 and AZD9466 (*Cluster 1 vs 3*). We found individual peptides that showed some specificity, including PRDM2 (amino acids 948–970), which was recruited by 4OHT, NCOA1 (amino acids 737–759), which was selectively dismissed by the three SERDs compared to 4OHT, and NRIP1 (amino acids

805–831), which was not dismissed by fulvestrant (**Fig. 2B**). While it is possible to identify peptides that are selective for these compounds (*16, 32*), most of the peptide interactions showed identical responses to the ligands in *Cluster 1*, with Pearson correlations (r) ≥ 0.90 between ligand-dependent peptide interactions (**Fig. 2B**).

Cluster 2 was in the same clade as *Cluster 1* and contained the E-ring piperidine-substituted compounds, as well as the compounds with F-ring Roussel and acrylate side chains, all of which showed less pronounced dismissal of the E2-induced peptide interactions than compounds in *cluster 1* (**Fig. 2A**). *Cluster 2* also has many more unique peptide interactions than *cluster 1*, reflected in lower Pearson correlations (r = 0.65–0.74 vs 4OHT). These included NCOR2 peptide (amino acids 649-671), which is derived from a protein with context-selective coactivator or corepressor activity (*33, 34*), and was dismissed by **16** and **20** but not 4OHT (**Fig. 2C**). C*luster 4* displayed peptide interaction patterns most different from the traditional antagonists, and included the compounds with F-ring piperidines, E-ring Roussel or acrylate side chains, and both the E- and F-ring substituted benzyl compounds. For example, **20** showed very little overlap in peptide interaction patterns with 4OHT and showed many peptides that were selective for **20** compared to 4OHT (**Fig. 2C**). The dual-mechanism inhibitors displayed a variety of different solution structural features that differentiate them from the traditional antagonists all of which displayed highly similar interaction profiles.

The ER-Y537S mutation changed the clustering pattern ligand-dependent peptide interactions. 4OHT, AZD9496, and GDC-0810 still clustered together and dismissed many of the same E2-induced peptide interactions (*Cluster 1*, **Fig. 2D**), while fulvestrant now clustered with [E]-Bn-1S (**29**) and [F]-RU-Ent2 (**27**) in *Cluster 2* from the same clade. Despite this clustering pattern, fulvestrant still displayed a higher Pearson correlation with 4OHT (**Fig. S5A**), as they strongly dismissing many of the peptides (**Fig. S5B–C**). The other major clade includes *Cluster 3*, which contains only [E]-OC_2-piperidine (**16**), and

Cluster 4, which contained all the remaining piperidine-containing compounds, the acrylates, as well as the [E]-RU (**14**) and [F]-Bn (**25**) compounds. The dramatic shift in peptide interaction patterns is underscored by **16**, which with the ER-Y537S displayed no overlapping effect on peptide interaction patterns with 4OHT (**Fig. 2E vs 2C**). These observations highlight the similarities in solution structures of ER-WT or ER-Y537S bound to the traditional direct antagonists, and conversely point to a range of novel solution structures for many of the dual-mechanism inhibitors, some of which are unique to the mutant ER-Y537S. Given that the surface structure controls the recruitment of transcriptional coactivators and corepressors as conveyers of receptor activity, these unique conformations likely contribute to the robust activity profiles of the dual-mechanism inhibitors.

Atypical side chains perturb the ERα LBD helix 12 conformation: Structural and HDX-Mass Spectrometry Studies

To further understand ligand-dependent effects on receptor structure, we compared X-ray crystal structures of ERα LBD complexes with dual-mechanism inhibitors and other antagonists. In the LBD, the [F]-OC_3-Pip (**20)** side chain exited towards h12 and in doing so also shifted h11 by 1.6 Å to induce indirect antagonism (**Fig. 3A**). Here, the piperidine head group made VDW contacts with Trp383 in the same location where Pro535 in the h11-h12 loop typically resides in contact with Trp383 (**Fig. S6A**). The **20-bbound** ER structure differed from that stabilized by SERMs such as raloxifene, as h12 was shifted 2.6 Å towards the C-terminus of h11, allowing Leu539 to directly contact the piperidine group of **20** (**Fig. 3B, Fig. S6A**). Unlike traditional SERM side chains that are stabilized by H-bonding, or the rigid acrylates of SERDs, the side chain of **20** is flexible with many degrees of freedom, suggesting that the shift in h12 is driven by both the shift in h11, which pulls on the h11-h12 loop, and additionally by the position of the atypical side chain. The

structure of the [E]-Bn (**29**)-bound LBD showed even more dramatic effects on h12, with very weak electron density where h12 was expected to be positioned, demonstrating that h12 was disordered (**Fig. 3C**). This is important, as the original two-position model of h12 (*7*) (**Fig. S1D** vs **F**) does not account for how certain antagonists recruit transcriptional corepressors. Structural and biochemical data demonstrate that the disordering or displacement of h12 renders a more open or accessible AF2 surface, which is required for binding of a longer 3 helical peptide motif found in corepressors (*8-10, 35*) to support a more complete antagonism of proliferation.

To validate the destabilizing effects of the ligands on the ER LBD in solution, we examined the dynamics of secondary structural elements through mass spectrometry analysis of the exchange of amide hydrogens for deuterium using mass spectrometry (HDX-MS) (*36*). These included the high affinity enantiomers of the parental compound **30** (the high affinity enantiomer of **13, Fig. 1A**), the F-ring-substituted Roussel side chain compound **27**, and the E-ring substituted benzyl compound **29**. While 4OHT and fulvestrant stabilized the C-terminal half of h11 proximal to the ligands, the parental OBHS-N **30 and** the dual-mechanism inhibitors **27** and **29** did not, consistent with indirect antagonism directed at h11 (**Fig. 3D, Fig. S6B**). All of the compounds stabilized helices 3 and h4 in the AF-2 surface, except for **29**, the compound that destabilized h12 in the crystal structure (**Fig. 3E**, **Fig. S6C**). With **27**, the extended hydrophobic Roussel side chain may directly contact the AF-2 surface to stabilize its secondary structural elements, as was seen with the fulvestrant analog, ICI 164,384 (*37*) (**Fig. S6D**). With the other compounds, the stabilization of the AF-2 surface is likely through h12 binding to the AF-2 surface in the inactive conformer (**Fig. S1F**) (*6, 7*), highlighting the ability of **29** to destabilize h12 in solution and in the crystal structure. These studies demonstrate that with indirect antagonism, the shifts in h11 destabilize or reposition h12 of the ER LBD, allowing the side chains to have distinct roles in stabilizing alternate conformers of h12.

Dual-mechanism inhibitors drive the formation of ERα conformational heterodimers

Helix 11 forms part of the dimer interface for ER, and also for other nuclear receptors that function as obligate heterodimers with the Retinoid X Receptor (RXR). Many of the dual-mechanism inhibitor structures were ligand-induced conformational heterodimers, where genetically identical monomers adopt different conformations in the context of the dimer, directed by ligand-induced allostery. With [F]-AcrEster (**21**) and [F]-Acr (**23**), the F-ring faced outward in one monomer and inward in the dimer partner (**Fig. 4A**), in the latter case hydrogen bonding to the base on h3 (**Fig. S7A**). With the F-ring inward conformation, h11 moves closer to its agonist-bound position where the His524-Leu525 backbone is 1.4 Å away from the position enforced by the outward F-ring conformer. The structure of GDC-810 revealed that the ligand formed an H-bond with h11-h12 loop to *pull* on h12 (**Fig. 7B**), rather than a typical SERM side chain-mediated *pushing* on the loop (*31*), but in the F-ring out binding mode the side chains of **21** and **23** were disordered. In fact, most of the structures showed conformational heterodimers, and many also had disordered side chains (**Fig. S7C-E**). Superimposing all nine new OBHS-N structures revealed a remarkable degree of conformational heterogeneity, with a range in the spatial positioning of the His524 and Leu525 h11 backbone of 3.4 Å (**Fig. 4B**). To quantitate the extent of conformational heterodimerization, we superimposed the B chains onto the A chains for each structure and a set of control structures and measured the distance between the chains for the backbone amides or sidechains of His524 and Leu525. The structures of tamoxifen and most published SERD-ER structures were crystallized as monomers, demonstrating that they stabilized identical monomers in the dimer, while raloxifene, E2, lasofoxifene and bazedoxifene showed almost identical dimers, with distances < 0.5Å (**Fig. 4C**). In contrast, most of the OBHS-N structures showed conformational heterogeneity

subunits in the dimer (**Fig. 4C**), with one monomer displaying greater indirect antagonism—shifts in h11 away from the agonist conformation.

To understand the mechanism of action causing conformational heterodimers, we examined the H-bond network bridging the dimer interface in the C-terminal half of h11 (**Fig. 4D**). While Glu521 and Lys520 can form a water-mediated electrostatic network across the dimer interface in the same plane of the ligand, this network was weak and highly variable. However, the Asn519-Asn519' H-bond was very strong and was stabilized by the adjacent His516 residues (**Fig. 4E**). The Asn519-Asn519' H-bond was kept within a very narrow range in our new structures and in a set of 62 published sub-2 Å ER structures (**Fig. 4E, Fig. S7F**). Further, if we generated by modeling conformational homodimers with our structures (A chain/A chain or B chain/B chain), the Asn519-Asn519' H-bonds became asymmetric, with the ~2.2 Å or 3.3 Å distances representing a clash and weak bond. These observations indicate that with these particular ligands this bond is transmitting allosteric information across an interface of two identical monomers that is conformationally heterodimeric. The binding of one ligand, here designed to shift/twist h11, orients h11 in the dimer partner into a unique conformer that guides the binding of the second ligand into a profoundly different binding mode, with its own associated activity profile.

The consequence of conformational heterodimer function is not just an ensemble of indirect antagonist conformers, but induced effects on h12. With [E]-Bn (**29**) bound ER, both sides of the dimer showed the F-ring facing out, but there was a 1 Å shift in h11 that was associated with a rotation of the ligand, placing the benzyl groups in different positions. When the benzyl group was closer to h3, h12 was disordered in Chain A, as we showed in **Fig. 3C**. However, with the rotation of the benzyl towards h11 in the B chain, the h11-h12 loop and h12 were pulled towards the benzyl until Pro535 docked against the benzyl group (**Fig. 3B–C**). Thus, the benzyl provides a docking platform for destabilizing h12

away from the AF2 surface, as we also observed with [F]-OC3-Pip (**20**) (**Fig. 3B**). The conformational heterodimers thus display the structural features of being bound to two "different" ligands that stabilize different conformers of the ligand and the ER LBD, which may drive unique biology, as for example seen with the combination treatment with bazedoxifene and conjugated estrogens (*38*).

Activity of dual mechanism inhibitors in allele-driven models antiestrogen resistance

A significant fraction of patients with recurrent ER+ breast cancers present with constitutively active ER mutations, including Y537S and D358G (*31, 39-41*), while de novo EGFR overexpression drives a worse outcome and tamoxifen resistance in a significant subset of newly presenting breast cancer patients (*21, 22*). We overexpressed EGFR in MCF-7 cells (**Fig. S8**), which we compared to MCF-7 cells engineered to express only ER-Y537S or ER-D538G (*40*). With these models we observed the expected loss of both potency and efficacy in response to 4OHT or fulvestrant, with the EGFR model showing the greatest loss of response to 4OHT (**Fig. 5A**). We tested our two high potency enantiomers, **27** and **29**, and two ligands with SERM-like properties (**16** and **20**) that showed unusual peptide binding (**Figure 2**) and structural features (**Fig. 3A-C, Fig. 4A–C**) and were highly efficacious in blocking Y537S reporter activity (**Fig 1I**). All of the ligands showed reduced efficacy, but **27** showed better potency in the mutant ERα models, while **20** and **29** showed slightly better potency in the EGFR resistance model (**Fig. 5B**). Despite their diverse side chains for direct antagonism, all of these compounds suppressed proliferation across resistance models, highlighting the important role of the dual mechanism for antagonizing ERα actions.

We developed the first structure-based design model of resistance for both tamoxifen and fulvestrant. We used the tamoxifen-bound ER structure to design L372S/L536S as a set of mutations to stabilize h12 as seen in that structure, docked into the AF2 surface, and showed that this blocked binding of the NCOR1 corepressor to ER and enforced AF1-dependent SERM agonist activity for tamoxifen (*23, 42*). Here, we demonstrate that this model also renders fulvestrant an agonist and test this model for compound profiling (**Fig. 5C–D**). In this context, all of the ligands were significantly more efficacious than 4OHT, except for the acrylates **23** and **24** and the [E]-OC_3-Pip (**16**) and [E]-OC_4-Pip (**17**) (**Fig. 5C–D**). Most of the compounds were also more efficacious than fulvestrant, including those with SERM like side chains, while the Roussel and benzyl side chain compounds were significantly more efficacious, almost completely blocking the AF1-driven activity that was enhanced by tamoxifen or fulvestrant (**Fig. 5C–D**).

DISCUSSION

In this work, we present dual-mechanism ER inhibitors (DMERI) as a flexible chemical platform for the generation of ligands with tailored SERM or SERD like properties that are broadly efficacious across different anti-estrogen resistance models, including a structure-based design model of tamoxifen and fulvestrant agonist activity (**Fig. 5**). The probe of ER solution structure with a library of interacting peptides and HDX revealed that traditional single mechanism inhibitors—whether SERM or SERD—overall stabilized very similar structures, while the DMERI imposed unique solution structures (**Fig. 2–3**). Our structural analyses demonstrated that these ligands induced unique perturbations to h11 and h12 to support their strong antagonism, including the formation of conformational heterodimers, where the receptor is in effect “reading” the same ligand in two different ways (**Fig. 3–4**). This is similar to how h11 can transmit information across the RXR heterodimer interface,

411 enabling the ligand on one side of the dimer to control the activity of the heterodimer
412 partner (*43*), but with genetically identical dimer partners.

413 Our findings stand in contrast to the traditional view of nuclear receptor allostery,
414 which is based on single, direct-acting mechanisms, and by which the ligand adopts a
415 single pose to control the conformation of the protein (**Fig. 6A-C**)(*44*). The single-
416 mechanism ligands select or induce lowest energy conformations of the receptor
417 associated with specific activity profiles that can be active, inactive, or tissue selective (**Fig.**
418 **6A–D**). The targeting of multiple antagonist sub-states that we can do with DMERIs may
419 provide a therapeutic targeting advantage similar to the effects of targeting multiple growth
420 pathways with combination therapies, or the combined use of bazedoxifene and
421 conjugated estrogens to achieve unique ER-mediated signaling characteristics (*38*).

422 A key feature of the OBHS-N scaffold is that the indirect antagonism drives full
423 antagonism comparable to fulvestrant, which we showed with the parental compounds
424 lacking a side chain (*23*). This then enabled the added side chains to take on different
425 functional roles. Since the development of tamoxifen in the 1970s and fulvestrant in the
426 1990s, the next generation SERMs and SERDs have directed either an aminoalkyl group
427 to push on the h11-h12 loop or the acrylate unit to pull on it, leading to series of compounds
428 with side chains that were localized around a very tight structural interface with ER. With
429 DMERI, the h11-h12 loop was pulled indirectly via h11 to destabilize h12. This enabled a
430 diversity of side chain activities from either the E-ring or F-ring to dial back in SERM activity
431 (**Fig. 1G**), bind directly to h12 to produce altered antagonist conformers (**Fig. 3B, Fig. 4F**),
432 or produce efficacy significantly greater than fulvestrant by fully destabilizing h12 with full
433 antagonists (**Fig. 3C, Fig. 3E**, **Fig. 5D**). This advance greatly expands the potential design
434 principals for the ligand side chain that is not being used as the primary driver of
435 antagonism and explains why we observed strong antagonism even when the side chain
436 did not engage in the known modes of antagonism or was completely disordered.

437 The stabilization of h12 that we observed in the absence of ligand with the Y537S
438 (*24*) blocks one of the routes for ligands to bind, leading to a general loss of potency across
439 compounds (**Fig 5A**)(*45, 46*). In this context the role of DMERI side chains is to effectively
440 displace h12, without necessarily interacting with the h11-12 loop, enabling alternative
441 chemistry focused on SERD or SERD activity profiles, potency, side effects, or
442 pharmacokinetic parameters. A critical shortcoming of the parental indirect antagonists
443 was lack of efficacy against the ER-Y537S mutant, which retained the agonist conformer
444 of h12 despite a 2.4 Å shift in h11(*23*), resulting in constitutive AF-2 activity (**Fig. 6E**). Here
445 we were able to identify four distinct side chains with efficacy comparable to fulvestrant in
446 targeting mutant ERs (**Fig. 5B**), highlighting the robustness of the DMERI platform.
447 The AF-2 constitutively activating mutations are found in many metastatic and
448 therapy resistant breast cancers, despite ER still being expressed (*3*). However, next
449 generation SERMs have not replaced tamoxifen for treatment of breast cancer due to
450 decades of safety data on tamoxifen, and we would argue lack of a targeted resistance
451 allele for newly presenting patient stratification. Hence, there is an unmet clinical need for
452 SERM compounds with efficacy against defined resistance alleles. Mutation,
453 overexpression, or amplification of EGFR signaling may be present in up to 1/3 of breast
454 cancers, where it is associated with lower ER expression, clinical tamoxifen resistance
455 and worse patient outcome (*21, 22*). In this regard, we note that several of our piperidine
456 compounds with some cell-type specific AF-1 activity were as effective as fulvestrant in
457 an EGFR overexpression model that was completely tamoxifen resistant (**Fig. 5A–B**).
458 Other forms of de novo resistance are associated with increased AF-1 activity,
459 including overexpression of interacting coregulators such as members of the NCOA1–3
460 genes, but also with phosphorylation of Ser305 by kinases involved in inflammatory,
461 growth factor, and cytoskeletal signaling (*30, 47-49*). We showed that Ser305 in the hinge
462 domain can H-bond to Arg548 just C-terminal to H12 and stabilize the SERM resistance

463 conformation with h12 docked in the AF-2 surface, enabling tamoxifen dependent AF-1
464 activity (*30*). The fulvestrant resistance model we have developed further stabilizes this
465 SERM agonist conformer by combining h3 L372S, designed from the tamoxifen-bound ER
466 structure (3ERT.pdb) to add an H-bond to h12 Asp545, with L536S, which removes the
467 unfavorable solvent exposed leucine and instead H-bonds to the base of h12 to stabilize
468 its helical structure. Importantly, mutations of L536 to histidine or arginine have appeared
469 in metastatic disease (*41*), which we predict act similarly to activate AF-1. The ER-
470 L372S/L536S double mutant thus presents the first structure-based design tool to study
471 tamoxifen and fulvestrant agonist activity, enabling the identification of ER ligands with
472 greater antagonism than fulvestrant (**Fig. 5C–D**). Combining two chemical targeting
473 approaches—direct and indirect antagonism—into a single ligand thus provides a flexible
474 platform for next generation ER-directed therapies with different targeted signaling
475 outcomes and broad efficacy across different treatment models.
476

477 **Acknowledgments.** NIH grant R01 CA220284 (KWN, TI, BSK, JAK), Breast Cancer
478 Research Foundation grant (BCRF-083 to BSK and BCRF-084 to JAK and BSK), NIH
479 Training grant GM 070421 (VSG), 345 Talent Project from Shengjing Hospital of China
480 Medical University China (SY). KWN is supported by the Frenchman's Creek Women for
481 Cancer Research
482

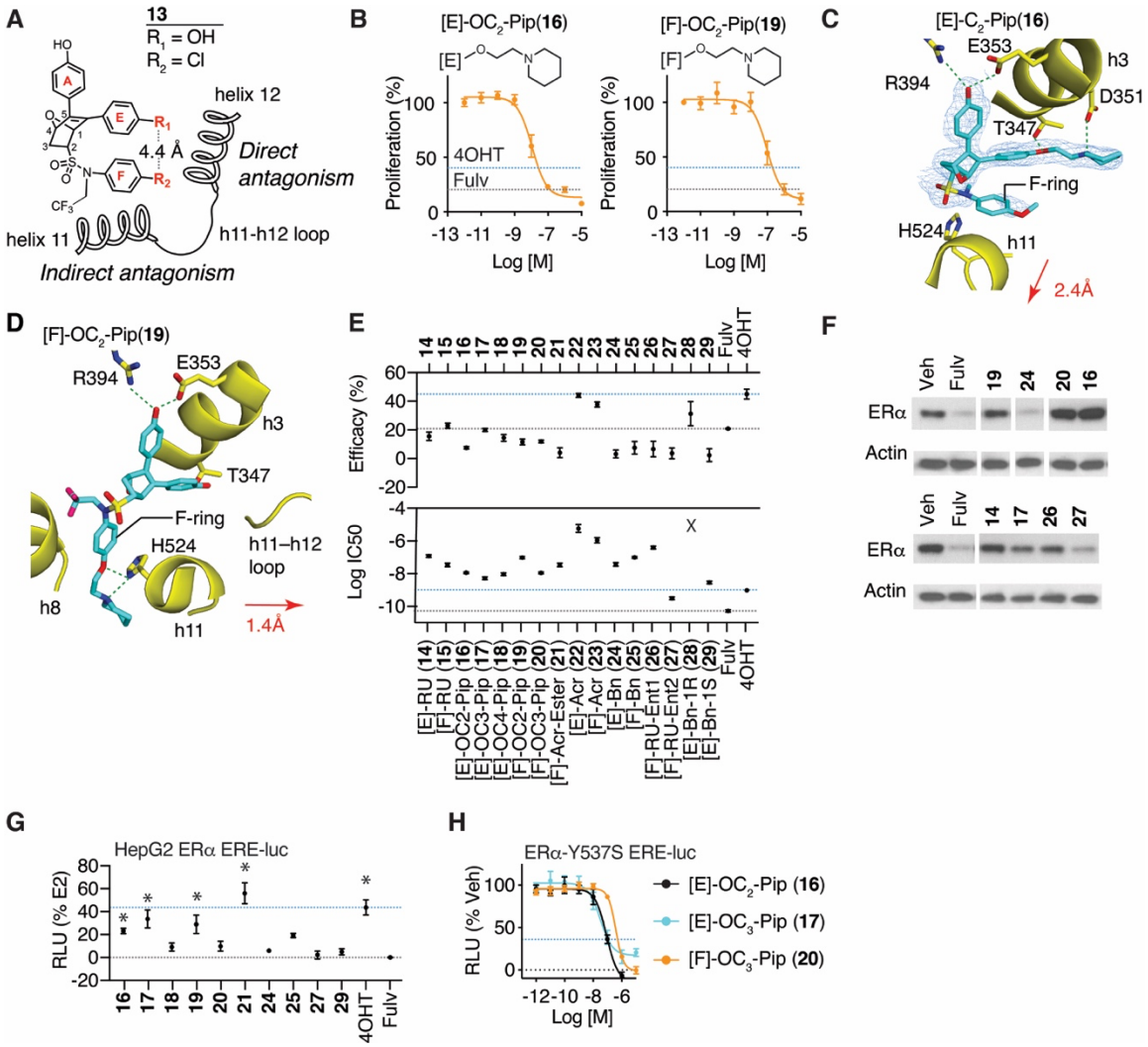

Figure 1. Dual-mechanism ER inhibitors fully suppress breast cancer cell proliferation.

A) Chemical structure of the OBHS-N scaffold and the orientation of substituents R_1 and R_2, with respect to h11 and h12 in the ER-LBD. (When R_1 has a substituent, R_2 is -OCH_3 group; when R_2 has a substituent, R_1 is –OH.)

B) Proliferation of MCF-7 cells treated for 5 days with 4OHT, fulvestrant (Fulv), or the indicated compounds. Datapoints are mean ± SEM, N= 6.

C) Structure of [E]-OC_2-Pip (**16**)-bound ER LBD showed the E-ring substituted piperidine H-bonding to Asp351 in helix 3 (h3), while the F-ring shifts helix 11 (h11) by 2.4 Å compared to an agonist bound structure. $2F_o$-F_c electron density map contoured to 1 σ.

D) Structure of [F]-OC_2-Pip (**19**)-bound ER LBD shows that its [F]-OC_2-Pip side chain exits the ligand-binding pocket between h8 and h11, H-bonds to His524, and shifts h11 towards h12.

E) Summary of dose response curves for compound inhibition of proliferation of MCF-7 cells, shown in **Figure S2A–H**. Datapoints are mean ± SEM, N= 6.

F) ER and β-actin levels in MCF-7 cells treated with the indicated compounds for 24 h. Whole cell lysates were analyzed by Western blot.

G) Summary of dose response curves for activation of ERα in 3xERE-luc assay in HepG2 cells. Datapoints are mean ± SEM, N= 3. *Significantly different from fulvestrant by 1-way ANOVA, Sidak's test adjusted p-value (p_{adj}) < 0.05. Dose curves are shown in **Figure S3B**.

H) Summary of dose response curves for inhibition of ERα-Y537S in 3xERE-luc assay in HEK293T cells. Datapoints are mean ± SEM, N= 3. Blue and black dashed lines indicate the maximal efficacies of 4OHT and Fulv, respectively.

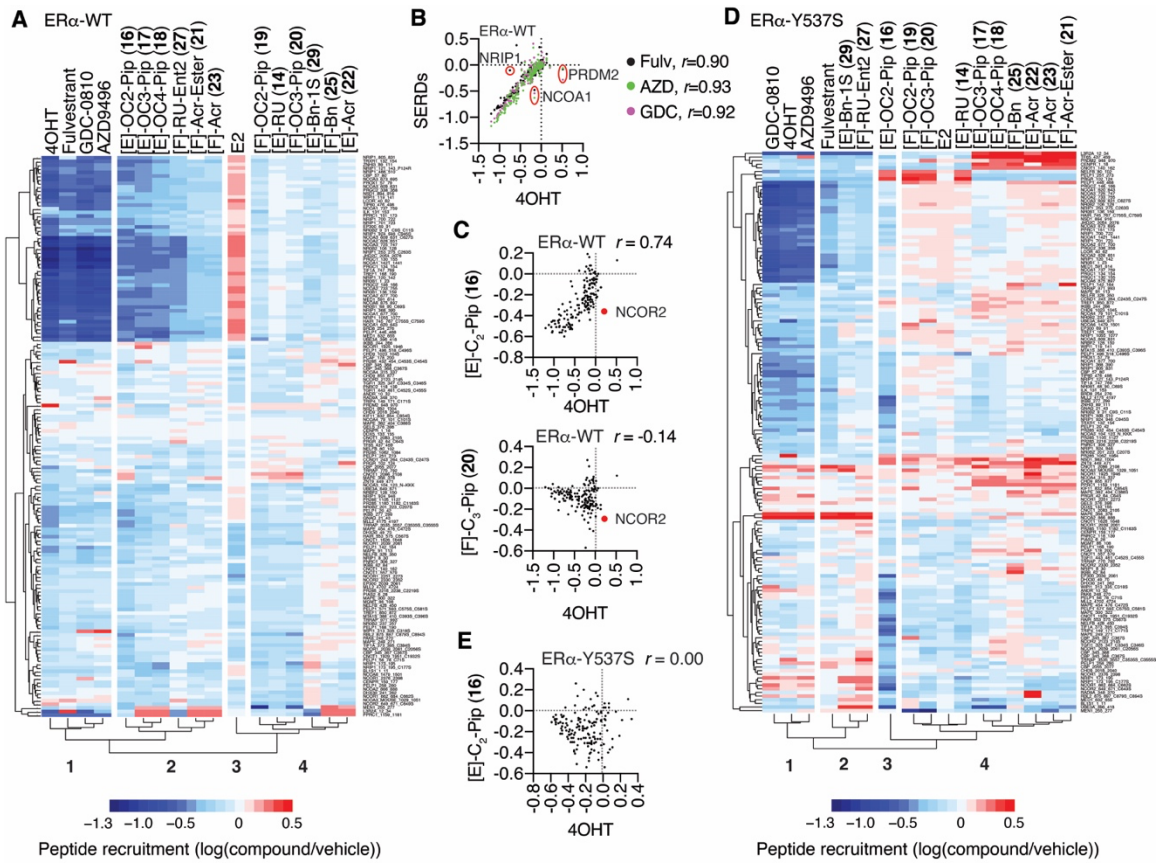

Figure 2. Dual-mechanism inhibitors promote conformations of ER that are distinct from traditional single mechanism inhibitors.

A) Hierarchical clustering of MARCoNI (Realtime Coregulator-Nuclear receptor Interaction) FRET assay for interaction of full-length, wild type (WT) ER with 154 peptides derived from nuclear receptor-interacting proteins and the indicated ligands.

B-C) MARCoNI Pearson correlations for 4OHT vs the indicated ligands. Fulvestrant (Fulv), GDC-0810 (GDC) or AZD9496 (ADZ). *r* = Pearson correlation ligand vs 4OHT

D) Hierarchical clustering of MARCONI data with ER-Y537S and the indicated ligands.

E) MARCoNI Pearson correlations for 4OHT vs [E]-C2-Pip (**16**) with the ER-Y537S. *r* = Pearson correlation.

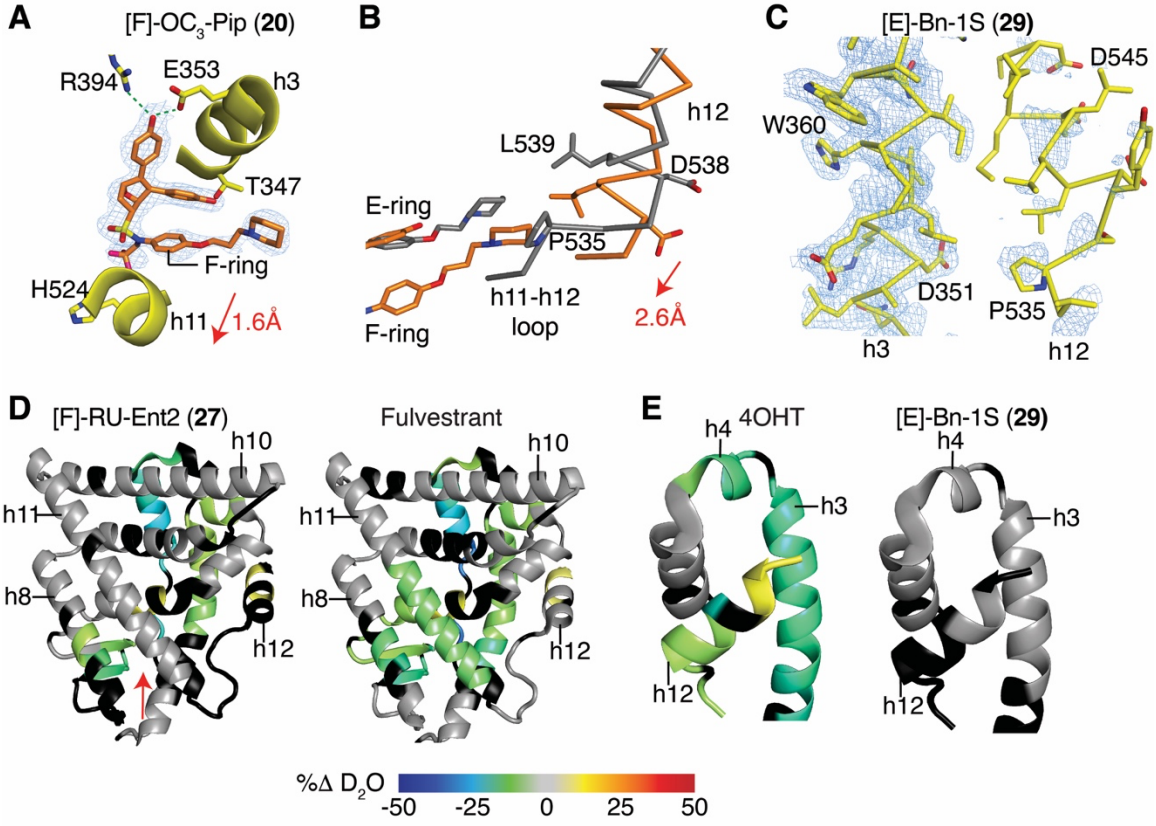

521

522 **Figure 3. Dual mechanism inhibitors destabilize helix 12**

523 **A**) Structure of the ER LBD bound to [F]-OC_3-Pip (**20**). $2F_o$-F_c electron density map
524 contoured at 1.0 σ shows the **20** F-ring facing outward between h3 and 11 towards h12,
525 shifting h11 1.6 Å compared to an agonist bound structure.

526 **B**) The structures of the ER LBD bound to **20** (coral) or raloxifene (gray) were
527 superimposed, showing the 2.6Å shift of h12 to contact the piperidine ring of **20**.

528 **C**) Structure of the ER LBD with [E]-Bn-1S (**29**) shows that h12 could not be modeled in 2
529 of 4 subunits due to poor electron density. The A chain is shown. The $2F_o$-F_c electron
530 density map is contoured at 1.0 σ.

D–E) Changes in ER-Y537S H/D exchange compared to the apo receptor. ERα-Y537S LBD was incubated with the indicated ligands and then assayed for exchange of amide hydrogens with deuterium over time, as measured by mass spectrometry.

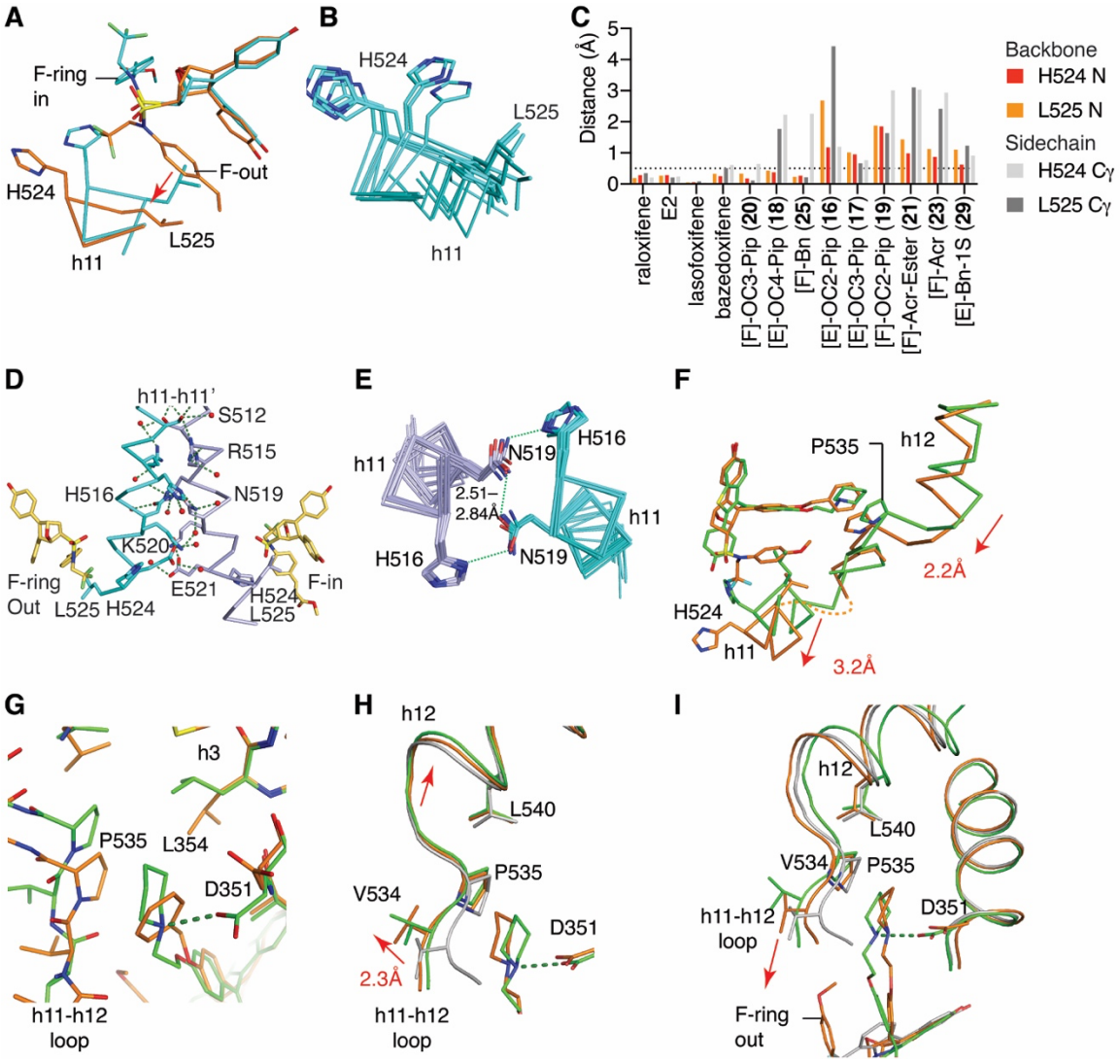

Figure 4. Dynamic ligands that bind in more than one orientation drive multiple antagonist conformers and the formation of conformational heterodimers

A) Structure of [F]-AcrEster (**21**)-bound ER showing different ligand binding positions in the dimeric subunits. The A and B chains were superimposed and colored blue or coral.

B) Nine structures of ERα bound to OBHS-N ligands were superimposed. Helix 11 residues 522-527 are shown as Cα trace. H524 Cα show a spatial range of 2.6 Å.

C) The B chains were superimposed on the A chains of ER structures with the indicated ligands. Distances between the indicated backbone amine (N) or sidechain Cγ were measured between the A and B chains for each structure.

D) A hydrogen bond network forms contacts across the C-terminal half of helices 11in the dimer interface. From structure of ERα bound to **21**.

E) Nine structures of ER with OBHS-N ligands were superimposed and h11 rendered as Cα traces. The N519-N519' H-bond is shown and is stabilized by adjacent His516 residues.

F) Structures of ER LBD subunits (B chains) bound to [E]-Bn-1S (**29**) (coral) or raloxifene (green) were superimposed, showing the C-terminus of h11, the h11-h12 loop, and h12 as C-α traces. The 3.2 Å shift in h11 pulled the h11-h12 loop and shifted h12 by 2.2 Å.

G) ER LBD subunits (B chains) bound to **29** (coral) or raloxifene (green) illustrates how the positioning of the benzyl supports the altered position of h12 through VDW contacts with Pro535 in the h11-h12 loop, as well as L354 and Asp351 in h3.

H–I) Structures of [E]-OC_2-Pip (**16**) (coral) and raloxifene (green)-bound ER were superimposed with another structure lacking an extended side chain (gray, A chain of 3OS8.pdb), showing the piperidine side chains and part of the h11-h12 loop and h12. **H**) The A chains are shown. **I**) The B chains are shown.

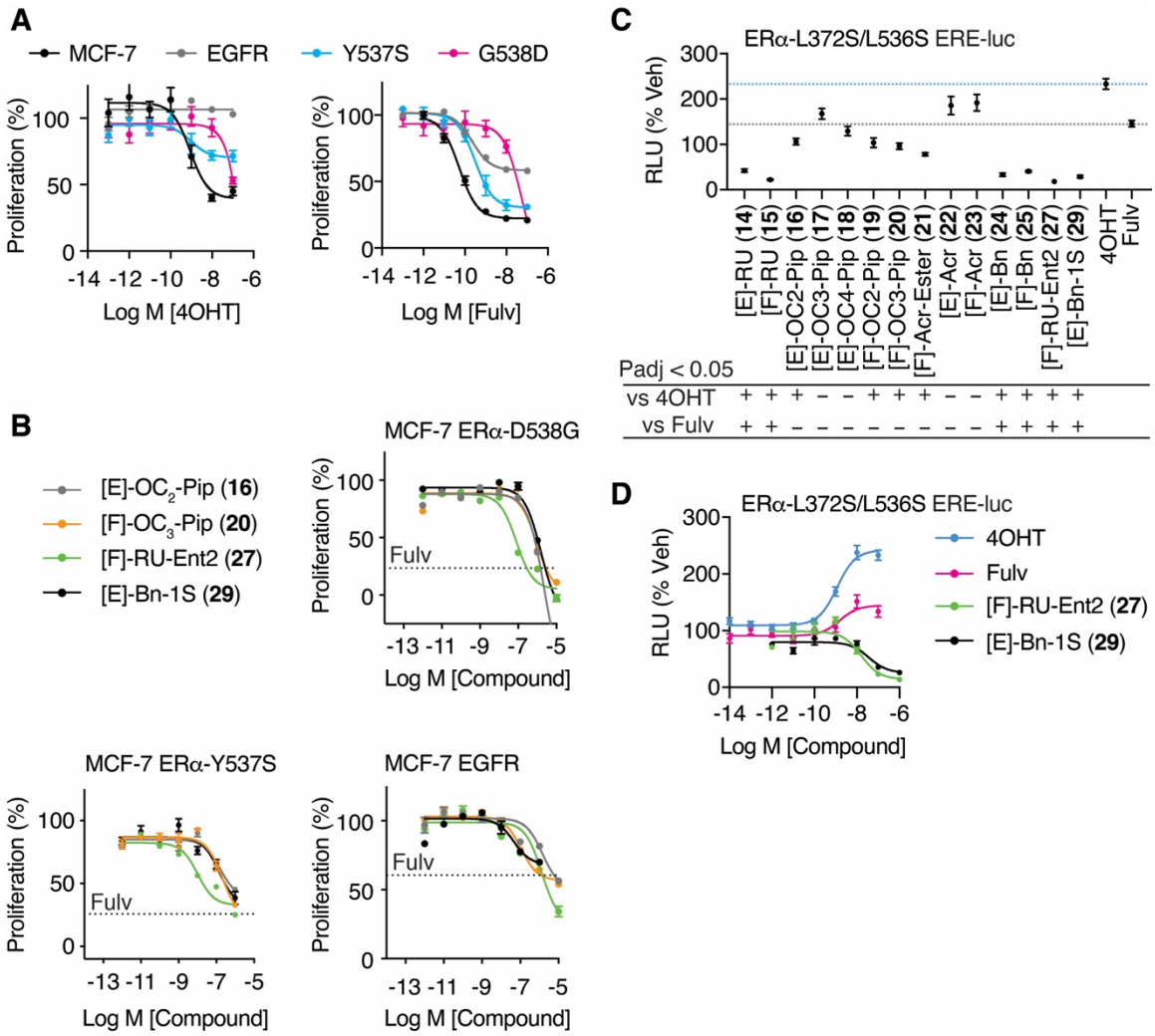

565

566 **Figure 5. Activity of ligands in allele-specific models of tamoxifen resistance.**

567 **(A)** WT MCF-7 cells and **(B)** MCF-7 cells engineered to express the mutant ERα-Y537S
568 or ERα-D538G, or overexpress EGFR, were treated with the indicated ligands for 5
569 days and analyzed for inhibition of cell proliferation. N = 3

570 **C–D)** Structure-based model of tamoxifen and fulvestrant resistance. HepG2 cells were
571 transfected with a 3xERE-luciferase reporter and ERα-L372S/L536S. The next day
572 cells were treated for 24 hr with the indicated ligands and processed for luciferase
573 activity. N = 6, except for 4OHT and Fulv where N=18. Data were analyzed by 1-way
574 ANOVA

575 Data are mean ± s.e.m.

576

577

578

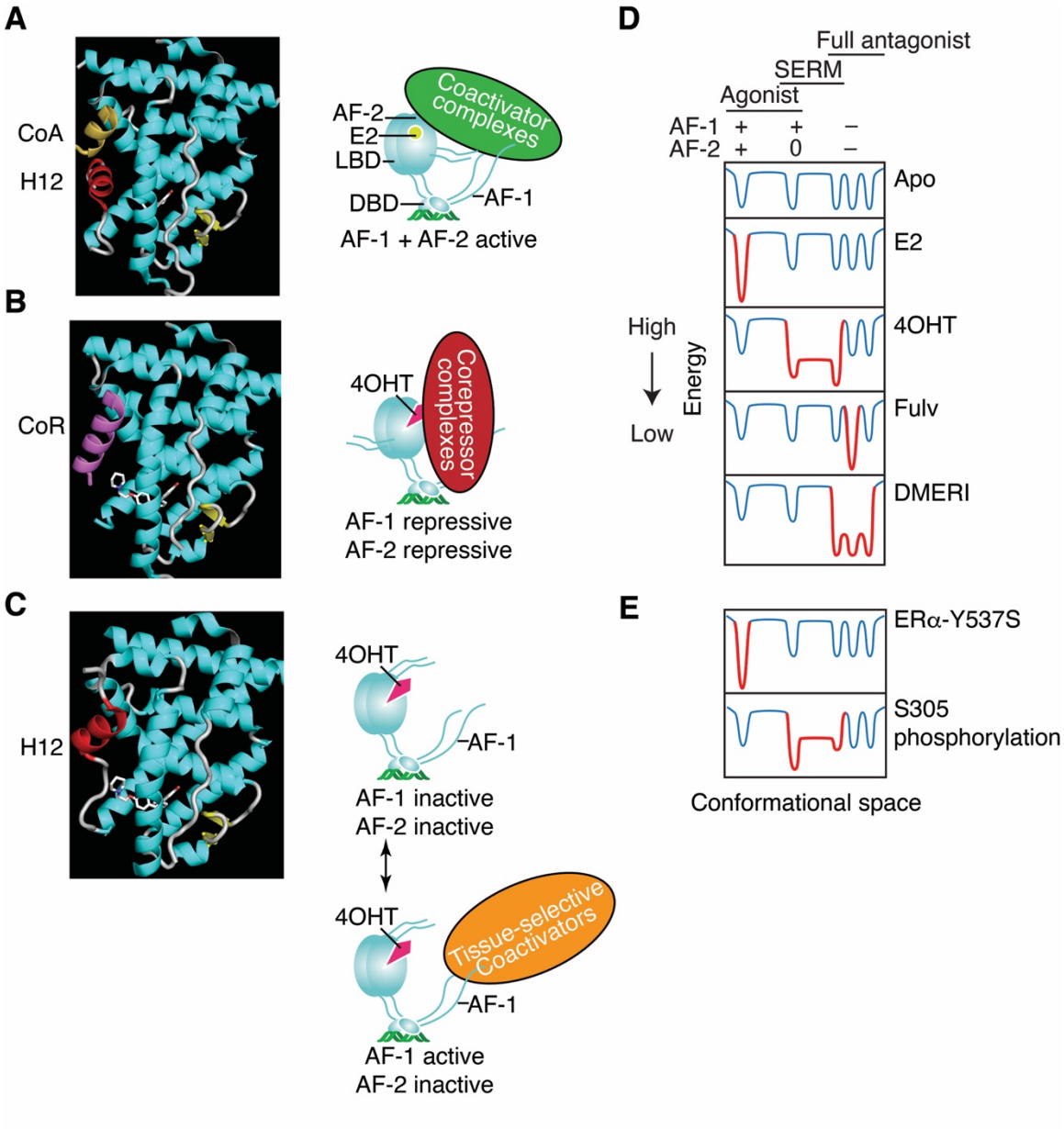

579

580 **Figure 6. Ligand-dependent control of ERα-LBD conformation, and of ER**

581 **coregulator recruitment and selection of activity states.**

A-C) three main conformers of the ER LBD are: an active conformer where agonists stabilize helix 12 (h12) to form one side of a binding site for transcriptional coregulators (*7*), called Activation Function-2 (AF-2); a repressive conformer where h12 is destabilized enabling recruitment of transcriptional corepressors that mediate chromatin condensation (*9, 12, 37, 50*); and an inactive conformer where h12 blocks both coactivators and corepressors(*7, 30*).

A) The active LBD conformation. *Left*, ribbon diagram of the ER LBD bound to estradiol. Helix 12 (h12, colored red) forms one side of the coactivator binding site, shown here binding to a peptide from Steroid Receptor Coactivator-2 (CoA colored yellow) 3UUD.pdb. *Right*, Schematic of ERα bound to estradiol (E2), DNA, and a coactivator complex. With full agonists, the coactivator recruitment to the LBD surface, AF-2 (Activation Function-2) nucleates binding of multi-protein coactivator complexes to other domains including AF-1 (Activation Function-1). DBD, DNA binding domain. Steroid Receptor Coactivators (SRCs) 1–3 bind to both AF-1 and AF-2 through separate interactions.

B) The transcriptionally repressive LBD conformation. *Left*, ribbon diagram of the ER LBD bound to a corepressor peptide, colored violet. When h12 is disordered by an antagonist, the LBD can bind an extended peptide motif found in transcriptional corepressors(*8*). 2JFA.pdb. *Right*, Cartoon of ERα bound to 4-hydroxytamoxifen (4OHT) and a corepressor complex, repressing both AF-1 and AF-2 activity and mediating mediate chromatin compaction and inhibition of proliferative gene expression.

C) The inactive LBD conformer. *Left*, Ribbon diagram of the ER LBD bound to an antagonist. Antagonists can flip h12 (colored red) into the coactivator/corepressor binding site, rendering the LBD inactive by blocking both coactivator and corepressor binding to

606 AF-2. 2QXS.pdb. *Right*, when h12 blocks both coactivators and corepressors from binding
607 the LBD, the activity of AF-1 is cell-type specific.

608 **D**) Energy diagram illustrating how ER ligands differ in stabilizing specific low energy
609 receptor conformations associated with transcriptional activity (+), inactivity (0), or
610 repression (–) that are being driven by the activity state of AF-2 or AF-1. The dips in the
611 curves represent different LBD conformations associated with the three AF-1/AF-2 activity
612 states shown at the top, *leftmost* being the active state ***(a)***, the *rightmost* representing sub-
613 states of the repressive state ***(b)***, and the *middle* the inactive state ***(c)***. When a state is
614 stabilized by a particular type of ligand, the curves become deeper, with gray changed to
615 red; the barrier heights between states indicate the ease of dynamic interchange among
616 the states or sub-states. The DMERI showed multiple mechanisms of antagonism,
617 represented by the multiple favored repressor sub-states with reduced exchange barriers.

618 **E**) ER-dependent tamoxifen resistance. Constitutively activating mutations such as ER-
619 Y537S stabilize the active conformer of AF-2(*24*). Phosphorylation of Ser305 in the hinge
620 domain enables an H-bond that stabilizes h12 in the inactive conformer, blocking
621 corepressors and enabling AF-1 activity (*30*).

622

623

METHODS

Cell Culture

MCF7, MCF7-ERα-Y537S, MCF7-ERα-D538G, HepG2, and MDA-MB231 cells were maintained in Dulbecco's modified eagle medium (DMEM) supplemented with 10% fetal bovine serum (FBS). MCF7-ERα-WT, MCF7-ERα-Y537S, MCF7-ERα-D538G were a gift from Steffi Oesterreich. The cells lines above were cultured with 1% penicillin/ streptomycin/ neomycin (PSN) antibiotics, 1% MEM non-essential amino acids, and 1% GlutaMAX (all from Gibco™ by Thermo Fisher Scientific), maintained at 37°C in a 5% CO_2 incubator. Cells were tested regularly for mycoplasma contamination.

Luciferase co-transfection assay

HepG2 cells were seeded in 10 cm plates containing 10 ml of DMEM (Gibco™ by Thermo Fisher Scientific, cat. no. 11995) supplemented with 10% fetal bovine serum (FBS), 1x GlutaMAX (Gibco™ by Thermo Fisher Scientific, cat. no. 35050061), 1x MEM nonessential amino acids (Corning,cat. no. 25-025-CI), 1x penicillin-streptomycin-neomycin (PSN) antibiotic mixture (Thermo Fisher Scientific, cat. no.15640055), and 2.5 µg/ml Plasmocin™ (Invivogen, cat. no. ant-mp). The next day, the cells were rinsed with 1x PBS and the medium was replaced with 10 ml of phenol red-free DMEM (Corning, cat. no. 17205CV) supplemented with 10% charcoal-stripped FBS (cs-FBS) (Thermo Fisher Scientific; cat no. A3382101). The cells were then co-transfected with 5.0 µg of 3xERE-Luc reporter plasmid and 0.5 µg of ERα (WT/mutant) expression plasmid using Fugene HD reagent (Promega, cat no. E2311).

After 24 h, the cells were resuspended in phenol red-free DMEM plus 10% cs-FBS, and transferred to a 384-well plate (Greiner Bio-One, cat. no. 781080) at a density of ~17,000 cells/well containing 25 µl of phenol red-free DMEM plus 10% cs-FBS. The next day, the test compounds were added using a Biomek NXP 100-nl pintool (Beckman Coulter, Inc.). The plates were sealed with Breathe-Easy permeable membranes (Diversified Biotech, cat. no. BEM-1), covered with stainless steel specimen plate lids (U.S. Patent 6,534,014), and incubated at 37°C overnight. Luciferase activity was measured 24 h later, using the britelite plus reporter gene assay system (PerkinElmer, cat no. 6066761) or the Bright-Glo™ Luciferase Assay System (Promega, cat no. E2620) and an Envision plate reader (PerkinElmer).

Cell Proliferation Assay

Cells were suspended in steroid-free media supplemented with 10% charcoal-stripped FBS and passed through a 30-micron strainer (Miltenyl Biotec, cat. no. 130-110-915). 25 µl of the cell suspension (i.e. 1,000 or 2,000 cells) was dispensed into each well of 384-well white, flat-bottom microplates (Greiner Bio-One CellStar, cat no. 781080), using a Martix WellMate Microplate Reagent Dispenser (Thermo Fisher Scientific). The next day, test compounds were added to the wells using a Biomek NXP 100-nl pintool (Beckman Coulter). The plates were sealed with Breathe-Easy permeable membranes (Diversified Biotech, Cat no. BEM-1), covered with a stainless steel specimen plate lid (U.S. Patent 6,534,014), and incubated at 37°C and 5% CO2. “Start plates” with replica wells were stored at -80°C to record the initial number of cells. After 5 days, the start plates were thawed for 15 min at 37°C, and the number of cells/well in all plates were compared. To this end, 25 µl of CellTiter-Glo® assay reagent (Promega, cat no. G7573) was added to each well using the Wellmate reagent dispenser. The plates were shaken gently at room

672 temperature for 5 min on an orbital shaker, and then allowed to sit for 5 min. Luminescence
673 was measured using an Envision plate reader (PerkinElmer). Proliferation data was
674 normalized using the initial number of cells as 0%, and the final number of cells in vehicle
675 (DMSO)-treated wells as 100%.

676

677 *Quantitative RT-PCR (qPCR)*

678 Total RNA was isolated using the RNeasy kit with on-column DNase I digest (QIAGEN).
679 4 µg total RNA samples were reverse-transcribed in 40 µl reactions using the High-
680 Capacity RNA-to-cDNA™ Kit (Thermo Fisher Scientific, cat. no. 4387406). cDNA samples
681 were analyzed by real-time PCR in triplicate 10 ul reactions using the 2X TaqMan® gene
682 expression master mix (Applied Biosystems™ by Thermo Fisher Scientific, cat. no.
683 4369016) with human *GREB1* (Hs00536409_m1) and *GAPDH* (Hs02758991_g1)
684 expression assays. Relative mRNA levels were compared using the ΔΔCt method.

685

686 *Western Blot*

687 Cells were lysed in ice-cold RIPA buffer (20 mM Tris pH 7.5, 150 mM NaCl, 1% NP40,
688 0.5% Sodium deoxycholate, 1 mM EDTA and 0.1% SDS). Protein samples were loaded
689 on Any kD™ Mini-PROTEAN® TGX™ Precast Protein Gels (Bio-rad, Hercules, CA) and
690 transferred onto PVDF membranes (Thermo Scientific, Rockford, IL). The membranes
691 were blocked with PBS-T + 5% nonfat dry milk and probed with primary antibodies
692 overnight. The next day, the membranes were washed with with TBS-T, and incubated
693 with HRP-conjugated probes (Santa Cruz Biotechnology) and developed using an ECL
694 detection system (GE Healthcare Bio-Sciences, Pittsburg, PA).

695

696 *Antibodies and Probes*

697 ERα (F-10) mouse mAb (1:1000, cat. no. sc-8002), ERα (H222) rat mAb (1:1000 dilution,
698 cat. no. sc-53492), β-Actin (C4) mouse mAb (1:10,000 dilution, cat. no., sc-47778), HRP-
699 conjugated mouse IgG kappa binding protein (cat. no., sc-516102), and HRP-conjugated
700 goat anti-rat IgG antibody (cat no. sc-2006), were purchased from Santa Cruz
701 Biotechnology, Inc.

702

703 *Macromolecular X-ray Crystallography*

704 The ERα-L372S/L536S double-mutant ligand-binding domain (LBD, amino acid residues
705 298–554) was expressed in BL21 (DE3) E. coli cells, purified by IMAC using a Ni2+
706 column, dialysis, TEV digest, ion exchange, and size exclusion chromatography to remove
707 the HA tag, as previously described(*24*). The purified LBD was co-crystallized with various
708 ligands through sitting drop vapor diffusion method using trial gradients of 20% –25% (w/v)
709 PEG 3350, 200 mM MgCl2, and pH 6.5–8.0, as previously described (*42, 51*). Data was
710 collected at the Stanford Synchrotron Radiation Lightsource (Beamline: 12-2) and
711 Advanced Photon Source (Beamlines: SER-CAT BM22, ID-22), both at temperature of
712 100 K and wavelength of 1.0 Å and scaled using AutoPROC (*52*) with the application of
713 STARANISO (Globalphasing) to accommodate anisotropic diffraction. The structures
714 were solved by molecular replacement of the starting model, 2QXS.pdb, and then rebuilt
715 and refined using the PHENIX software suite version 1.16 (*53, 54*). Ligand restraints were
716 built on the PHENIX electronic Ligand Builder and Optimisation Workbench (*55*). Ligand
717 docking was automated with LigandFit in Phenix and visually inspected using COOT
718 version 0.8.9.2, as previously described (*56, 57*). New structures were further refined on

719 the PDB-REDO server (*58*), before final refinement and validation in the PHENIX
720 environment. Structures were analyzed using COOT and imaged using PyMOL
721 (Schrodinger).

722

723 *MARCoNI coregulator interaction profiling*

724 Microarray assay for real-time nuclear receptor coregulator interaction (MARCoNI) was
725 performed as previously described (*59*). In short, a PamChip peptide micro array with 154
726 unique coregulator-derived NR interaction motifs (#88101, PamGene International) was
727 incubated with his-tagged ERα LBD in the presence of 10 μM compound or solvent only
728 (2% DMSO, apo). Receptor binding to each peptide on the array was detected using
729 fluorescently labeled his-antibody, recorded by CCD and quantified. Per compound, three
730 technical replicates (arrays) were analyzed to calculate the log-fold change (modulation
731 index, MI) of each receptor-peptide interaction versus apo. Significance of this modulation
732 was assessed by Student's t-Test.

733

734 *Hydrogen-Deuterium Exchange (HDX) detected by mass spectrometry (MS)*

735 Differential HDX-MS experiments were conducted as previously described with a few
736 modifications(*60*).
737 **Peptide Identification:** Peptides were identified using tandem MS (MS/MS) with an
738 Orbitrap mass spectrometer (Q Exactive, ThermoFisher). Product ion spectra were
739 acquired in data-dependent mode with the top five most abundant ions selected for the
740 product ion analysis per scan event. The MS/MS data files were submitted to Mascot
741 (Matrix Science) for peptide identification. Peptides included in the HDX analysis peptide
742 set had a MASCOT score greater than 20 and the MS/MS spectra were verified by manual

743 inspection. The MASCOT search was repeated against a decoy (reverse) sequence and
744 ambiguous identifications were ruled out and not included in the HDX peptide set.
745 **HDX-MS analysis:** Protein (10 μM) was incubated with the respective ligands at a 1:10
746 protein-to-ligand molar ratio for 1 h at room temperature. Next, 5 μl of sample was diluted
747 into 20 μl D_2O buffer (20 mM Tris-HCl, pH 7.4; 150 mM NaCl; 2 mM DTT) and incubated
748 for various time points (0, 10, 60, 300, and 900 s) at 4°C. The deuterium exchange was
749 then slowed by mixing with 25 μl of cold (4°C) 3 M urea and 1% trifluoroacetic acid.
750 Quenched samples were immediately injected into the HDX platform. Upon injection,
751 samples were passed through an immobilized pepsin column (2mm × 2cm) at 200 μl
752 min^{-1} and the digested peptides were captured on a 2mm × 1cm C_8 trap column (Agilent)
753 and desalted. Peptides were separated across a 2.1mm × 5cm C_{18} column (1.9 μl
754 Hypersil Gold, ThermoFisher) with a linear gradient of 4% - 40% CH_3CN and 0.3% formic
755 acid, over 5 min. Sample handling, protein digestion and peptide
756 separation were conducted at 4°C. Mass spectrometric data were acquired using an
757 Orbitrap mass spectrometer (Exactive, ThermoFisher). HDX analyses were performed in
758 triplicate, with single preparations of each protein ligand complex. The intensity weighted
759 mean m/z centroid value of each peptide envelope was calculated and subsequently
760 converted into a percentage of deuterium incorporation. This is accomplished determining
761 the observed averages of the undeuterated and fully deuterated spectra and using the
762 conventional formula described elsewhere(*61*). Statistical significance for the differential
763 HDX data is determined by an unpaired t-test for each time point, a procedure that is
764 integrated into the HDX Workbench software(*62*). Corrections for back-exchange were
765 made on the basis of an estimated 70% deuterium recovery, and accounting for the known
766 80% deuterium content of the deuterium exchange buffer.

Data Rendering: The HDX data from all overlapping peptides were consolidated to individual amino acid values using a residue averaging approach. Briefly, for each residue, the deuterium incorporation values and peptide lengths from all overlapping peptides were assembled. A weighting function was applied in which shorter peptides were weighted more heavily and longer peptides were weighted less. Each of the weighted deuterium incorporation values were then averaged to produce a single value for each amino acid. The initial two residues of each peptide, as well as prolines, were omitted from the calculations. This approach is similar to that previously described (*63*). HDX analyses were performed in triplicate, with single preparations of each purified protein/complex. Statistical significance for the differential HDX data is determined by t test for each time point, and is integrated into the HDX Workbench software (*62*).

REFERENCES

1. H. S. Rugo, R. B. Rumble, E. Macrae, D. L. Barton, H. K. Connolly, M. N. Dickler, L. Fallowfield, B. Fowble, J. N. Ingle, M. Jahanzeb, S. R. D. Johnston, L. A. Korde, J. L. Khatcheressian, R. S. Mehta, H. B. Muss, H. J. Burstein, Endocrine Therapy for Hormone Receptor–Positive Metastatic Breast Cancer: American Society of Clinical Oncology Guideline. *Journal of Clinical Oncology* **34**, 3069-3103 (2016).
2. K. Tryfonidis, D. Zardavas, B. S. Katzenellenbogen, M. Piccart, Endocrine treatment in breast cancer: Cure, resistance and beyond. *Cancer Treatment Reviews* **50**, 68-81 (2016).
3. R. Clarke, J. J. Tyson, J. M. Dixon, Endocrine resistance in breast cancer--An overview and update. *Mol Cell Endocrinol* **418 Pt 3**, 220-234 (2015).
4. H. J. Lerner, P. R. Band, L. Israel, B. S. Leung, Phase II study of tamoxifen: report of 74 patients with stage IV breast cancer. *Cancer Treat Rep* **60**, 1431-1435 (1976).

5. V. C. Jordan, E. Phelps, J. U. Lindgren, Effects of anti-estrogens on bone in castrated and intact female rats. *Breast Cancer Res Treat* **10**, 31-35 (1987).

6. A. M. Brzozowski, A. C. W. Pike, Z. Dauter, R. E. Hubbard, T. Bonn, O. Engstrom, L. Ohman, G. L. Greene, J.-A. Gustafsson, M. Carlquist, Molecular basis of agonism and antagonism in the oestrogen receptor. *Nature* **389**, 753-758 (1997).

7. A. K. Shiau, D. Barstad, P. M. Loria, L. Cheng, P. J. Kushner, D. A. Agard, G. L. Greene, The structural basis of estrogen receptor/coactivator recognition and the antagonism of this interaction by tamoxifen. *Cell* **95**, 927-937 (1998).

8. H. J. Huang, J. D. Norris, D. P. McDonnell, Identification of a negative regulatory surface within estrogen receptor alpha provides evidence in support of a role for corepressors in regulating cellular responses to agonists and antagonists. *Mol Endocrinol* **16**, 1778-1792 (2002).

9. P. Webb, P. Nguyen, P. J. Kushner, Differential SERM effects on corepressor binding dictate ERalpha activity in vivo. *J Biol Chem* **278**, 6912-6920 (2003).

10. N. Heldring, T. Pawson, D. McDonnell, E. Treuter, J. A. Gustafsson, A. C. Pike, Structural insights into corepressor recognition by antagonist-bound estrogen receptors. *J Biol Chem* **282**, 10449-10455 (2007).

11. D. J. DeFriend, A. Howell, R. I. Nicholson, E. Anderson, M. Dowsett, R. E. Mansel, R. W. Blamey, N. J. Bundred, J. F. Robertson, C. Saunders, et al., Investigation of a new pure antiestrogen (ICI 182780) in women with primary breast cancer. *Cancer research* **54**, 408-414 (1994).

12. J. Guan, W. Zhou, M. Hafner, R. A. Blake, C. Chalouni, I. P. Chen, T. De Bruyn, J. M. Giltnane, S. J. Hartman, A. Heidersbach, R. Houtman, E. Ingalla, L. Kategaya, T. Kleinheinz, J. Li, S. E. Martin, Z. Modrusan, M. Nannini, J. Oeh, S. Ubhayakar, X. Wang, I. E. Wertz, A. Young, M. Yu, D. Sampath, J. H. Hager, L. S. Friedman,

817 A. Daemen, C. Metcalfe, Therapeutic Ligands Antagonize Estrogen Receptor
818 Function by Impairing Its Mobility. *Cell* **178**, 949-963 e918 (2019).
819 13. S. E. Wardell, J. R. Marks, D. P. McDonnell, The turnover of estrogen receptor
820 alpha by the selective estrogen receptor degrader (SERD) fulvestrant is a
821 saturable process that is not required for antagonist efficacy. *Biochem Pharmacol*
822 **82**, 122-130 (2011).
823 14. S. E. Wardell, A. P. Yllanes, C. A. Chao, Y. Bae, K. J. Andreano, T. K. Desautels,
824 K. A. Heetderks, J. T. Blitzer, J. D. Norris, D. P. McDonnell, Pharmacokinetic and
825 pharmacodynamic analysis of fulvestrant in preclinical models of breast cancer to
826 assess the importance of its estrogen receptor-alpha degrader activity in antitumor
827 efficacy. *Breast Cancer Res Treat* **179**, 67-77 (2020).
828 15. C. De Savi, R. H. Bradbury, A. A. Rabow, R. A. Norman, C. de Almeida, D. M.
829 Andrews, P. Ballard, D. Buttar, R. J. Callis, G. S. Currie, J. O. Curwen, C. D. Davies,
830 C. S. Donald, L. J. Feron, H. Gingell, S. C. Glossop, B. R. Hayter, S. Hussain, G.
831 Karoutchi, S. G. Lamont, P. MacFaul, T. A. Moss, S. E. Pearson, M. Tonge, G. E.
832 Walker, H. M. Weir, Z. Wilson, Optimization of a Novel Binding Motif to (E)-3-(3,5-
833 Difluoro-4-((1R,3R)-2-(2-fluoro-2-methylpropyl)-3-methyl-2,3,4,9-tetra hydro-1H-
834 pyrido[3,4-b]indol-1-yl)phenyl)acrylic Acid (AZD9496), a Potent and Orally
835 Bioavailable Selective Estrogen Receptor Downregulator and Antagonist. *Journal*
836 *of medicinal chemistry* **58**, 8128-8140 (2015).
837 16. J. D. Joseph, B. Darimont, W. Zhou, A. Arrazate, A. Young, E. Ingalla, K. Walter,
838 R. A. Blake, J. Nonomiya, Z. Guan, L. Kategaya, S. P. Govek, A. G. Lai, M.
839 Kahraman, D. Brigham, J. Sensintaffar, N. Lu, G. Shao, J. Qian, K. Grillot, M. Moon,
840 R. Prudente, E. Bischoff, K. J. Lee, C. Bonnefous, K. L. Douglas, J. D. Julien, J. Y.
841 Nagasawa, A. Aparicio, J. Kaufman, B. Haley, J. M. Giltnane, I. E. Wertz, M. R.
842 Lackner, M. A. Nannini, D. Sampath, L. Schwarz, H. C. Manning, M. N. Tantawy,

C. L. Arteaga, R. A. Heyman, P. J. Rix, L. Friedman, N. D. Smith, C. Metcalfe, J. H. Hager, The selective estrogen receptor downregulator GDC-0810 is efficacious in diverse models of ER+ breast cancer. *eLife* **5**, 1-34 (2016).

17. B. Zhang, J. R. Kiefer, R. A. Blake, J. H. Chang, S. Hartman, E. R. Ingalla, T. Kleinheinz, V. Mody, M. Nannini, D. F. Ortwine, Y. Ran, A. Sambrone, D. Sampath, M. Vinogradova, Y. Zhong, J. C. Nwachukwu, K. W. Nettles, T. Lai, J. Liao, X. Zheng, H. Chen, X. Wang, J. Liang, Unexpected equivalent potency of a constrained chromene enantiomeric pair rationalized by co-crystal structures in complex with estrogen receptor alpha. *Bioorg Med Chem Lett* **29**, 905-911 (2019).

18. G. S. Tria, T. Abrams, J. Baird, H. E. Burks, B. Firestone, L. A. Gaither, L. G. Hamann, G. He, C. A. Kirby, S. Kim, F. Lombardo, K. J. Macchi, D. P. McDonnell, Y. Mishina, J. D. Norris, J. Nunez, C. Springer, Y. Sun, N. M. Thomsen, C. Wang, J. Wang, B. Yu, C. L. Tiong-Yip, S. Peukert, Discovery of LSZ102, a Potent, Orally Bioavailable Selective Estrogen Receptor Degrader (SERD) for the Treatment of Estrogen Receptor Positive Breast Cancer. *Journal of medicinal chemistry* **61**, 2837-2864 (2018).

19. S. W. Fanning, L. Hodges-Gallagher, D. C. Myles, R. Sun, C. E. Fowler, I. N. Plant, B. D. Green, C. L. Harmon, G. L. Greene, P. J. Kushner, Specific stereochemistry of OP-1074 disrupts estrogen receptor alpha helix 12 and confers pure antiestrogenic activity. *Nat Commun* **9**, 2368 (2018).

20. S. W. Fanning, G. L. Greene, Next-Generation ERalpha Inhibitors for Endocrine-Resistant ER+ Breast Cancer. *Endocrinology* **160**, 759-769 (2019).

21. S. Tsutsui, S. Ohno, S. Murakami, Y. Hachitanda, S. Oda, Prognostic value of epidermal growth factor receptor (EGFR) and its relationship to the estrogen receptor status in 1029 patients with breast cancer. *Breast Cancer Res Treat* **71**, 67-75 (2002).

869 22. S. Nicholson, J. R. Sainsbury, P. Halcrow, P. Chambers, J. R. Farndon, A. L. Harris,
870 Expression of epidermal growth factor receptors associated with lack of response
871 to endocrine therapy in recurrent breast cancer. *Lancet* **1**, 182-185 (1989).
872 23. S. Srinivasan, J. C. Nwachukwu, N. E. Bruno, V. Dharmarajan, D. Goswami, I.
873 Kastrati, S. Novick, J. Nowak, V. Cavett, H. B. Zhou, N. Boonmuen, Y. Zhao, J.
874 Min, J. Frasor, B. S. Katzenellenbogen, P. R. Griffin, J. A. Katzenellenbogen, K.
875 W. Nettles, Full antagonism of the estrogen receptor without a prototypical ligand
876 side chain. *Nature chemical biology* **13**, 111-118 (2017).
877 24. K. W. Nettles, J. B. Bruning, G. Gil, J. Nowak, S. K. Sharma, J. B. Hahm, K. Kulp,
878 R. B. Hochberg, H. Zhou, J. A. Katzenellenbogen, B. S. Katzenellenbogen, Y. Kim,
879 A. Joachmiak, G. L. Greene, NFkappaB selectivity of estrogen receptor ligands
880 revealed by comparative crystallographic analyses. *Nature chemical biology* **4**,
881 241-247 (2008).
882 25. J. Min, V. S. Guillen, A. Sharma, Y. Zhao, Y. Ziegler, P. Gong, C. G. Mayne, S.
883 Srinivasan, S. H. Kim, K. E. Carlson, K. W. Nettles, B. S. Katzenellenbogen, J. A.
884 Katzenellenbogen, Adamantyl Antiestrogens with Novel Side Chains Reveal a
885 Spectrum of Activities in Suppressing Estrogen Receptor Mediated Activities in
886 Breast Cancer Cells. *Journal of medicinal chemistry* **60**, 6321-6336 (2017).
887 26. S. Fanning, L. Hodges-Gallagher, D. Myles, R. Sun, C. Fowler, I. Plant, B. Green,
888 C. Harmon, G. Greene, P. Kushner, Specific stereochemistry of OP-1074 disrupts
889 estrogen receptor alpha helix 12 and confers pure antiestrogenic activity. *Nature*
890 *communications* **9**, 1-12 (2018).
891 27. S. Y. Dai, M. J. Chalmers, J. Bruning, K. S. Bramlett, H. E. Osborne, C. Montrose-
892 Rafizadeh, R. J. Barr, Y. Wang, M. Wang, T. P. Burris, Prediction of the tissue-
893 specificity of selective estrogen receptor modulators by using a single biochemical
894 method. *Proceedings of the National Academy of Sciences* **105**, 7171-7176 (2008).

28. R. Xiong, J. Zhao, L. M. Gutgesell, Y. Wang, S. Lee, B. Karumudi, H. Zhao, Y. Lu, D. A. Tonetti, G. R. Thatcher, Novel Selective Estrogen Receptor Downregulators (SERDs) Developed against Treatment-Resistant Breast Cancer. *Journal of medicinal chemistry* **60**, 1325-1342 (2017).

29. M. van Kruchten, E. G. de Vries, A. W. Glaudemans, M. C. van Lanschot, M. van Faassen, I. P. Kema, M. Brown, C. P. Schroder, E. F. de Vries, G. A. Hospers, Measuring residual estrogen receptor availability during fulvestrant therapy in patients with metastatic breast cancer. *Cancer Discov* **5**, 72-81 (2015).

30. J. D. Stender, J. C. Nwachukwu, I. Kastrati, Y. Kim, T. Strid, M. Yakir, S. Srinivasan, J. Nowak, T. Izard, E. S. Rangarajan, K. E. Carlson, J. A. Katzenellenbogen, X. Q. Yao, B. J. Grant, H. S. Leong, C. Y. Lin, J. Frasor, K. W. Nettles, C. K. Glass, Structural and Molecular Mechanisms of Cytokine-Mediated Endocrine Resistance in Human Breast Cancer Cells. *Mol Cell* **65**, 1122-1135 e1125 (2017).

31. S. W. Fanning, R. Jeselsohn, V. Dharmarajan, C. G. Mayne, M. Karimi, G. Buchwalter, R. Houtman, W. Toy, C. E. Fowler, R. Han, M. Laine, K. E. Carlson, T. A. Martin, J. Nowak, J. C. Nwachukwu, D. J. Hosfield, S. Chandarlapaty, E. Tajkhorshid, K. W. Nettles, P. R. Griffin, Y. Shen, J. A. Katzenellenbogen, M. Brown, G. L. Greene, The SERM/SERD bazedoxifene disrupts ESR1 helix 12 to overcome acquired hormone resistance in breast cancer cells. *eLife* **7**, (2018).

32. C. E. Connor, J. D. Norris, G. Broadwater, T. M. Willson, M. M. Gottardis, M. W. Dewhirst, D. P. McDonnell, Circumventing tamoxifen resistance in breast cancers using antiestrogens that induce unique conformational changes in the estrogen receptor. *Cancer research* **61**, 2917-2922 (2001).

33. J. K. Blackmore, S. Karmakar, G. Gu, V. Chaubal, L. Wang, W. Li, C. L. Smith, The SMRT coregulator enhances growth of estrogen receptor-alpha-positive

breast cancer cells by promotion of cell cycle progression and inhibition of apoptosis. *Endocrinology* **155**, 3251-3261 (2014).

34. C. L. Smith, I. Migliaccio, V. Chaubal, M. F. Wu, M. C. Pace, R. Hartmaier, S. Jiang, D. P. Edwards, M. C. Gutierrez, S. G. Hilsenbeck, S. Oesterreich, Elevated nuclear expression of the SMRT corepressor in breast cancer is associated with earlier tumor recurrence. *Breast Cancer Res Treat* **136**, 253-265 (2012).

35. H. E. Xu, T. B. Stanley, V. G. Montana, M. H. Lambert, B. G. Shearer, J. E. Cobb, D. D. McKee, C. M. Galardi, K. D. Plunket, R. T. Nolte, D. J. Parks, J. T. Moore, S. A. Kliewer, T. M. Willson, J. B. Stimmel, Structural basis for antagonist-mediated recruitment of nuclear co-repressors by PPARalpha. *Nature* **415**, 813-817 (2002).

36. S. Y. Dai, M. J. Chalmers, J. Bruning, K. S. Bramlett, H. E. Osborne, C. Montrose-Rafizadeh, R. J. Barr, Y. Wang, M. Wang, T. P. Burris, J. A. Dodge, P. R. Griffin, Prediction of the tissue-specificity of selective estrogen receptor modulators by using a single biochemical method. *Proceedings of the National Academy of Sciences of the United States of America* **105**, 7171-7176 (2008).

37. A. C. Pike, A. M. Brzozowski, J. Walton, R. E. Hubbard, A. G. Thorsell, Y. L. Li, J. A. Gustafsson, M. Carlquist, Structural insights into the mode of action of a pure antiestrogen. *Structure* **9**, 145-153 (2001).

38. J. H. Pickar, M. Boucher, D. Morgenstern, Tissue selective estrogen complex (TSEC): a review. *Menopause* **25**, 1033-1045 (2018).

39. S. W. Fanning, C. G. Mayne, V. Dharmarajan, K. E. Carlson, T. A. Martin, S. J. Novick, W. Toy, B. Green, S. Panchamukhi, B. S. Katzenellenbogen, E. Tajkhorshid, P. R. Griffin, Y. Shen, S. Chandarlapaty, J. A. Katzenellenbogen, G. L. Greene, Estrogen receptor alpha somatic mutations Y537S and D538G confer breast cancer endocrine resistance by stabilizing the activating function-2 binding conformation. *eLife* **5**, (2016).

40. A. Bahreini, Z. Li, P. Wang, K. M. Levine, N. Tasdemir, L. Cao, H. M. Weir, S. L. Puhalla, N. E. Davidson, A. M. Stern, D. Chu, B. H. Park, A. V. Lee, S. Oesterreich, Mutation site and context dependent effects of ESR1 mutation in genome-edited breast cancer cell models. *Breast Cancer Res* **19**, 60 (2017).

41. W. Toy, H. Weir, P. Razavi, M. Lawson, A. U. Goeppert, A. M. Mazzola, A. Smith, J. Wilson, C. Morrow, W. L. Wong, E. De Stanchina, K. E. Carlson, T. S. Martin, S. Uddin, Z. Li, S. Fanning, J. A. Katzenellenbogen, G. Greene, J. Baselga, S. Chandarlapaty, Activating ESR1 Mutations Differentially Affect the Efficacy of ER Antagonists. *Cancer Discov* **7**, 277-287 (2017).

42. J. B. Bruning, A. A. Parent, G. Gil, M. Zhao, J. Nowak, M. C. Pace, C. L. Smith, P. V. Afonine, P. D. Adams, J. A. Katzenellenbogen, K. W. Nettles, Coupling of receptor conformation and ligand orientation determine graded activity. *Nature chemical biology* **6**, 837-843 (2010).

43. D. J. Kojetin, E. Matta-Camacho, T. S. Hughes, S. Srinivasan, J. C. Nwachukwu, V. Cavett, J. Nowak, M. J. Chalmers, D. P. Marciano, T. M. Kamenecka, A. I. Shulman, M. Rance, P. R. Griffin, J. B. Bruning, K. W. Nettles, Structural mechanism for signal transduction in RXR nuclear receptor heterodimers. *Nat Commun* **6**, 8013 (2015).

44. K. W. Nettles, G. L. Greene, Ligand control of coregulator recruitment to nuclear receptors. *Annu Rev Physiol* **67**, 309-333 (2005).

45. K. E. Carlson, I. Choi, A. Gee, B. S. Katzenellenbogen, J. A. Katzenellenbogen, Altered ligand binding properties and enhanced stability of a constitutively active estrogen receptor: evidence that an open pocket conformation is required for ligand interaction. *Biochemistry* **36**, 14897-14905 (1997).

46. J. A. Katzenellenbogen, C. G. Mayne, B. S. Katzenellenbogen, G. L. Greene, S. Chandarlapaty, Structural underpinnings of oestrogen receptor mutations in endocrine therapy resistance. *Nature Reviews Cancer* **18**, 377-388 (2018).

47. C. Bentin Toaldo, X. Alexi, K. Beelen, M. Kok, M. Hauptmann, M. Jansen, E. Berns, J. Neefjes, S. Linn, R. Michalides, W. Zwart, Protein Kinase A-induced tamoxifen resistance is mediated by anchoring protein AKAP13. *BMC Cancer* **15**, 588 (2015).

48. J. Bostner, L. Skoog, T. Fornander, B. Nordenskjold, O. Stal, Estrogen receptor-alpha phosphorylation at serine 305, nuclear p21-activated kinase 1 expression, and response to tamoxifen in postmenopausal breast cancer. *Clin Cancer Res* **16**, 1624-1633 (2010).

49. I. Kastrati, S. Semina, B. Gordon, E. Smart, Insights into how phosphorylation of estrogen receptor at serine 305 modulates tamoxifen activity in breast cancer. *Mol Cell Endocrinol* **483**, 97-101 (2019).

50. T. Traboulsi, M. El Ezzy, V. Dumeaux, E. Audemard, S. Mader, Role of SUMOylation in differential ERalpha transcriptional repression by tamoxifen and fulvestrant in breast cancer cells. *Oncogene* **38**, 1019-1037 (2019).

51. N. Sharma, K. E. Carlson, J. C. Nwachukwu, S. Srinivasan, A. Sharma, K. W. Nettles, J. A. Katzenellenbogen, Exploring the Structural Compliancy versus Specificity of the Estrogen Receptor Using Isomeric Three-Dimensional Ligands. *ACS Chem Biol* **12**, 494-503 (2017).

52. C. Vonrhein, C. Flensburg, P. Keller, A. Sharff, O. Smart, W. Paciorek, T. Womack, G. Bricogne, Data processing and analysis with the autoPROC toolbox. *Acta Crystallogr D Biol Crystallogr* **67**, 293-302 (2011).

53. P. D. Adams, P. V. Afonine, G. Bunkoczi, V. B. Chen, N. Echols, J. J. Headd, L. W. Hung, S. Jain, G. J. Kapral, R. W. Grosse Kunstleve, A. J. McCoy, N. W. Moriarty, R. D. Oeffner, R. J. Read, D. C. Richardson, J. S. Richardson, T. C.

Terwilliger, P. H. Zwart, The Phenix software for automated determination of macromolecular structures. *Methods* **55**, 94-106 (2011).

54. J. C. Nwachukwu, M. R. Southern, J. R. Kiefer, P. V. Afonine, P. D. Adams, T. C. Terwilliger, K. W. Nettles, Improved crystallographic structures using extensive combinatorial refinement. *Structure* **21**, 1923-1930 (2013).

55. N. W. Moriarty, R. W. Grosse-Kunstleve, P. D. Adams, electronic Ligand Builder and Optimization Workbench (eLBOW): a tool for ligand coordinate and restraint generation. *Acta Crystallogr D Biol Crystallogr* **65**, 1074-1080 (2009).

56. P. Emsley, K. Cowtan, Coot: model-building tools for molecular graphics. *Acta Crystallogr D Biol Crystallogr* **60**, 2126-2132 (2004).

57. J. E. Debreczeni, P. Emsley, Handling ligands with Coot. *Acta Crystallogr D Biol Crystallogr* **68**, 425-430 (2012).

58. R. P. Joosten, F. Long, G. N. Murshudov, A. Perrakis, The PDB_REDO server for macromolecular structure model optimization. *IUCrJ* **1**, 213-220 (2014).

59. J. M. Aarts, S. Wang, R. Houtman, R. M. van Beuningen, W. M. Westerink, B. J. Van De Waart, I. M. Rietjens, T. F. Bovee, Robust array-based coregulator binding assay predicting ERalpha-agonist potency and generating binding profiles reflecting ligand structure. *Chem Res Toxicol* **26**, 336-346 (2013).

60. M. J. Chalmers, S. A. Busby, B. D. Pascal, Y. He, C. L. Hendrickson, A. G. Marshall, P. R. Griffin, Probing protein ligand interactions by automated hydrogen/deuterium exchange mass spectrometry. *Anal. Chem.* **78**, 1005-1014 (2006).

61. Z. Zhang, D. L. Smith, Determination of amide hydrogen exchange by mass spectrometry: a new tool for protein structure elucidation. *Protein science : a publication of the Protein Society* **2**, 522-531 (1993).

62. B. D. Pascal, S. Willis, J. L. Lauer, R. R. Landgraf, G. M. West, D. Marciano, S. Novick, D. Goswami, M. J. Chalmers, P. R. Griffin, HDX workbench: software for

the analysis of H/D exchange MS data. *J Am Soc Mass Spectrom* **23**, 1512-1521 (2012).

63. T. R. Keppel, D. D. Weis, Mapping residual structure in intrinsically disordered proteins at residue resolution using millisecond hydrogen/deuterium exchange and residue averaging. *J. Am. Soc. Mass Spectrom.* **26**, 547-554 (2015).